

Electrochemical Study of the Pt Nanoparticles Size Effect in the Formic Acid Oxidation

F. Godínez-Salomón, E. Arce-Estrada* and M. Hallen-López

Departamento de Ingeniería Metalúrgica, IPN-ESIQIE, UPALM Edif. 7, Zacatenco, México DF 07738, Mexico

*E-mail: earce@ipn.mx

Received: 26 January 2012 / Accepted: 18 February 2012 / Published: 1 March 2012

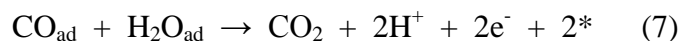
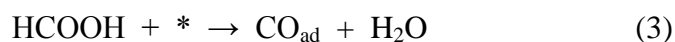
Cyclic voltammetry (CV) and electrochemical impedance spectroscopy (EIS) provided interesting information about the particle size effect during HCOOH electro-oxidation. They were evaluated Pt nanoparticles between 1.5 and 3.7 nm (From Etek Co.). Formic acid reaction shows strong particle size effect, which was correlated with surface condition. CV showed that under certain conditions small particles might have a better catalytic activity than the larger ones. The latter, was supported by EIS which indicate a higher blockage of active sites on larger particle. The co-adsorption of formate and CO on Pt have been postulated as the species which poisoning the catalyst's active sites inhibiting the oxidation of formic acid. The surface blockage was observed as a negative differential resistance (NDR) response. The potential from which NDR appears is higher when the nanoparticles sizes of Pt decrease due to a less effective inhibition process.

Keywords: Metals, electrochemical techniques, electrochemical properties.

1. INTRODUCTION

The oxidation of formic acid on platinum has been extensively investigated as a model reaction [1], furthermore, it shows interesting properties as a potential energy source for portable electronic devices [2]. Theoretically, direct formic acid fuel cells (DFAFC) present a higher electromotive force (EMF) than that of the hydrogen/oxygen or direct methanol fuel cells, in addition, this device runs well at high formic acid concentration because of slower permeation through Nafion[®] which decreases the *crossover* phenomenon [3]. These features make the DFAFC a serious candidate for practical applications. In this way, a well understanding of the fundamental processes occurring during operation is of great interest to develop better catalysts and enhance the fuel cell performance. It is

widely accepted that the electro-oxidation of formic acid to CO₂ follows the so-called “*dual-pathway*” mechanism [4,5]. In the direct path, a short-lived intermediate reactant commonly associated to formate specie has been proposed [6] (reactions 1-2). In the indirect path is proposed a mechanism in which a poisoning intermediate (CO) is formed and strongly adsorbed on the platinum surface (reaction 3). Adsorbed CO is oxidizing to CO₂ at high potentials by the reaction with the surface bonded HO_{ad} (reactions 4-5) or adsorbed H₂O (reactions 6-7).



The catalysts commonly used on fuel cells are composed of small noble metal particles (1-10 nm) dispersed on appropriate supports [7]. Changes in particle size have strong correlation with catalytic activities; several reports in the literature have shown a strong variation on the reaction rate or selectivity with the characteristics dimension of metallic clusters for different reactions, the so-called *particle size effect* [8]. Change on electrocatalytic properties can be related in general to two kinds of parameters: *electronic* and *geometric factors*. Electronics factors are mainly related to the surface electronic structure which can modify the binding energy of adsorbed species [9]. On the other hand, geometric factors are related to the topography of the atoms distribution on the surface, the presence of defect sites or agglomeration [10-12].

Taking into account the aforementioned, the goal of the present work is to study the Pt nanoparticles size effect in the range of 1.5-3.7 nm over the oxidation kinetics of formic acid, considering the dual mechanism already proposed. The electrocatalytic activity was monitored by cyclic voltammetry and electrochemical impedance spectroscopy.

2. EXPERIMENTAL

2.1. Electrocatalysts

They were used five different Pt high surface area catalysts supported on carbon Vulcan XC-72 (supplied by Etek Co.). According to the supplier, the Pt nanoparticles have mean diameters of 1.5, 2.0, 2.2, 2.9 and 3.7 nm.

2.2. Electrochemical measurements

The electrochemical evaluations were performed using rotating disc electrode (RDE) technique [14]. The preparation of the working electrode (WE) was carried out as follows: 50 mg of the corresponding Pt/C catalyst (1.5-3.7 nm) and 1 mL of Nafion[®] (5 % wt) were dispersed ultrasonically in 5 mL of ultrapure water (18.2 M Ω cm). 2 μ L of the catalyst ink was added onto a polished gold electrode (geometrical area 0.0314 cm²) and the film was dried by argon flow leading to a Pt loading between 26-318 μ g_{Pt} cm⁻². Afterwards the electrode was transferred to the electrochemical cell protected by a drop of ultrapure water. The WE immersion in the electrolyte solution was carried out under potential control at 0.05 V. The electrochemical measurements were conducted at room temperature in a conventional three-electrodes test cell filled with supporting electrolyte 0.1 M H₂SO₄ and HCOOH (0, 0.1 and 1.0 M) using a potentiostat/galvanostat PGSTAT 3600. The electrolyte solutions were prepared with Elga water (18.2 M Ω .cm, TOC < 3 ppb), H₂SO₄ (sigma-Aldrich \geq 98 %) and formic acid > 98 %. Before to electrochemical experiments, the oxygen of the solution was removed by bubbling high purity Ar (6.0-MTI 99.999%) at least 5 minutes. A Pt foil was used as counter-electrode and potentials were determined using an Ag/AgCl/KCl_{sat} reference electrode (0.256 V/NHE). All potentials, however, were reported in terms of the reversible hydrogen electrode (RHE) scale. The electrochemical impedance spectroscopy (EIS) measurements were performed step manner every 0.1 V from 0.35V to 1.15 V /RHE. It was used a frequency range from 10 kHz to 0.1 Hz, with an ac signal perturbation of 10 mV. After each EIS acquisition, a CV was done in the same solution to eliminate traces of the previous measurement, and the new test potential was restored and left there for 500 s for equilibration.

3. RESULTS AND DISCUSSION

3.1. Cyclic voltammetry

Figure 1a shows the cyclic voltammograms of Pt/C with different particles sizes in 0.1 M H₂SO₄ electrolyte solution, which was previously bubbled with argon to remove the oxygen. The curves showed three different potential regions according to polycrystalline platinum [14]. The hydrogen underpotential deposition domain (H_{upd}), between 0.05 and 0.4 V, exhibited relevant changes as a function of size. As particle size increases (e.g. 1.5-3.7 nm), it was observed a better definition of peaks around 0.144 V and 0.270 V. The latter was associated to changes in the distribution of surface atoms on the (111) and (100) crystal faces, as well on the edge and corner sites [9]. The potential range between 0.4 V and \sim 0.8 V correspond to “double layer” region. The presented width peak here observed was attributed to the quinone/hydro-quinone equilibrium owing to the carbon support [16]. Above \sim 0.8 V, surface oxide formation take place, but a relationship between particle sizes and surface oxide formation is not so clear. This effect was clearly defined in the reverse scan, where the oxide reduction potential was shifted toward a more negative value as the particle size decreases (Figure 1b). This is in agreement with results reported previously [17-20], and holds that the ophilicity of Pt nanoparticles increase by decreasing particle size.

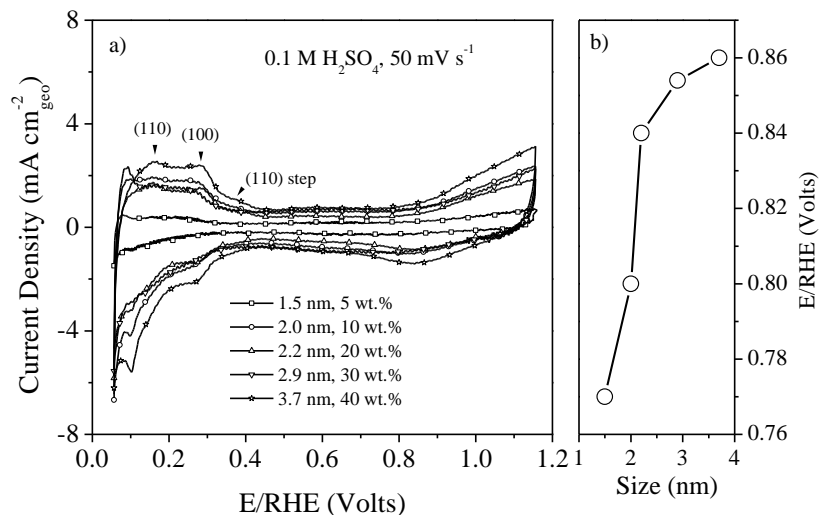


Figure 1. a) Cyclic voltammograms of Pt carbon supported catalysts samples recorded in 0.1 M H₂SO₄ solution at room temperature and scan rate 50 mV s⁻¹. b) Effect of particle size on potential of oxide reduction peaks.

3.2. Formic Acid Electro-oxidation and particle size effect

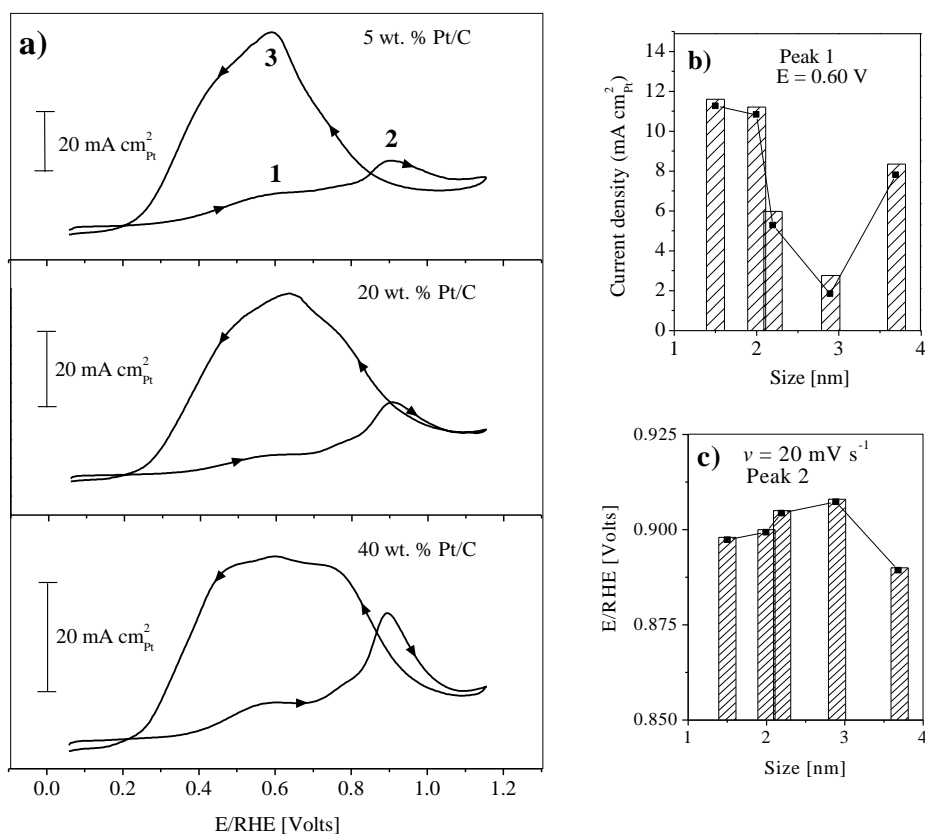


Figure 2. a) Cyclic voltammograms (20 mV s⁻¹) for electro-oxidation of 0.1 M HCOOH + 0.5 M H₂SO₄ on different particle sizes. Current density behavior of peak 1 at E = 0.6 V. (b) oxidation potential of peak 2 related to CO stripping and (c) versus catalysts loading, respectively.

Figure 2a shows representative cyclic voltammograms obtained for the electro-oxidation of 0.1 M formic acid in 0.5 M H₂SO₄ with particle diameters in the range of 1.5-3.7 nm. These voltammograms present the current density based on the specific surface area determined from the hydrogen desorption charge, assuming a coulometric charge of 210 $\mu\text{C cm}^{-2}$ [21].

Qualitatively, the shape of CV's was quite similar regardless particle size, rather, the voltammetric behavior is consistent with earlier studies reported on polycrystalline Pt surfaces [22, 23]. In general, the CVs showed three different potential regions marked as 1-3, in agreement with the order as they appeared. During the forward scan, the current density in the hydrogen region (H_{upd} , $E \leq 0.4$ V), are greatly suppressed. This behavior has been correlated with the poisoning of surface by the presence of CO_{ad} , formed through the chemical formic acid decomposition [24]. As the potential rising ($0.4 \leq E \leq 0.7$ V), is observed a slight increase in the current density which was higher on smaller particles (Figure 2b). Previous reports have demonstrated that this slight increase correspond to the oxidation of formic acid on the active sites released, by the oxidation of small amount of the adsorbed CO [25-27]. Despite unclarity in the voltammograms (Figure 2a), a small current decay is observed at the positive side of the peak (1). This phenomenon is caused by the appearance of a negative differential resistance (NDR), which has been related to adsorption of both CO and formate ion species [33], however this statement will be discussed below.

Above ~ 0.7 V, the reaction becomes significantly accelerated, attaining an anodic peak between 0.9 and 1.0 V depending on particle size (peak 2c). At higher potential, the appearing of non-reactive surface oxides [28] deactivates Pt. During the backward scan, the surface remains inactive until partial reduction of the Pt surface oxides takes place. Then, the current density suddenly increases due to the formic acid oxidation on Pt sites unblocked by oxygen species (peak 3). Below 0.4 V, the current decreases and drops to nearly zero, because of the surface poisoning by the accumulation of CO_{ad} [28, 29].

Considering from a qualitatively point of view, the similarity between voltammograms curves during formic acid oxidation, leads us suppose that the reaction mechanism is independent of the particle size. However, the difference of the current densities and the peak potentials (peaks 1-3), suggest some divergences on the kinetic process, respect to the particles size. Commonly, different surface processes such as adsorption/desorption, diffusion and electrochemical processes, have a strongly structure sensitivity and at the same time, this phenomenon could be linked with the particle size [12, 30].

3.3. Electrochemical impedance studies

Further studies of the electro-oxidation of HCOOH were carried out by electrochemical impedance measurements. Figure 3 shows typical Nyquist complex-plane impedance spectra of different supported Pt catalysts in 1.0 M HCOOH + 0.5 M H₂SO₄ with varied electrode potentials. The Nyquist-plot semicircles, were correlated with a faradic process involving a reaction-kinetic resistance in parallel with the non-ideal double layer capacitance element. The overall process is represented in

an equivalent circuit (Figure 5) and the fitted results data are summarized in Table 1. The impedance spectra showed an interesting dependence respect to electrode potential and particle size.

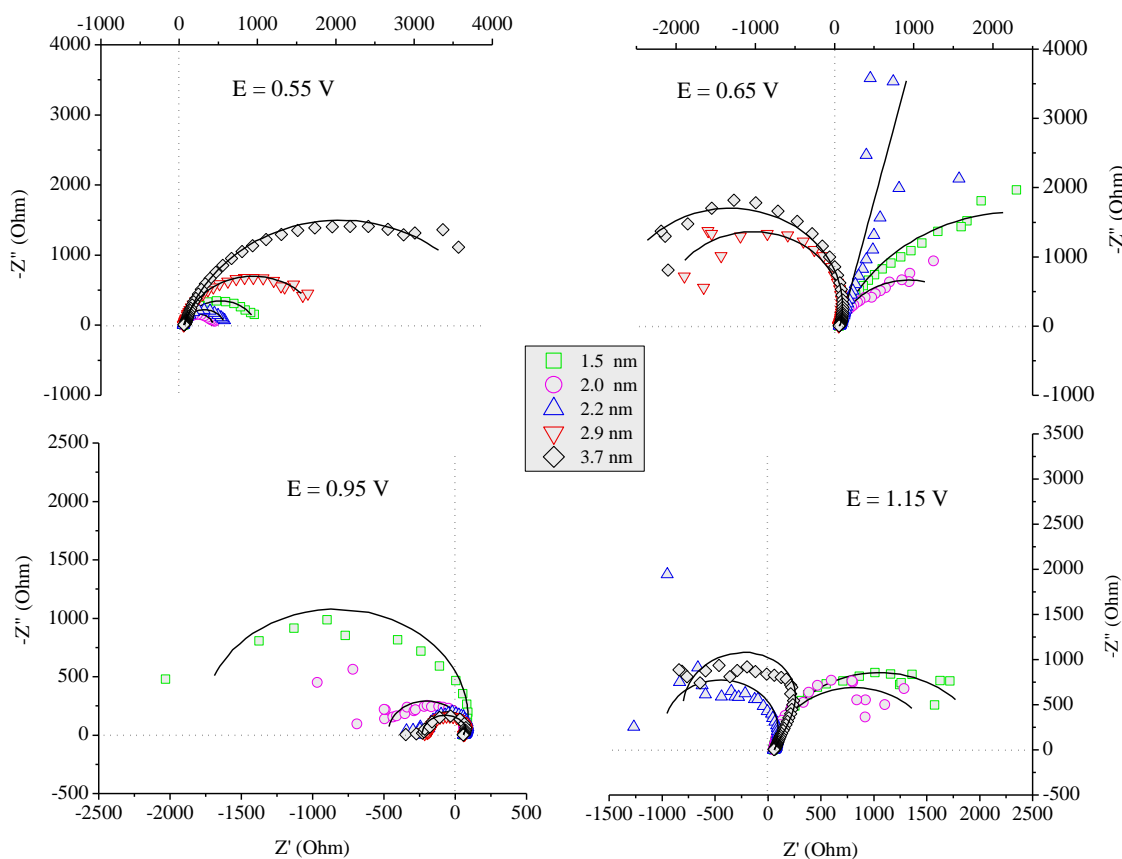


Figure 3. Complex-plane electrochemical impedance plots (Nyquist plots) for different platinum supported catalysts (1.5 to 3.7 nm) in 1.0 M HCOOH + 0.1 M H₂SO₄ electrolyte solution, at various electrode potentials. The solid lines represent the result of the fitting procedure to the experimental data by the equivalent circuit of Figure 5.

Table 1. Fitting parameters of the electrochemical impedance for the electro-oxidation of formic acid on platinum supported catalysts (particle size 1.5 to 3.7 nm) in various potentials (0.35 – 1.15 V/RHE).

E/V	Pt 5% (1.5 nm)			Pt 10% (2.0 nm)			Pt 20% (2.2 nm)		
	R _{CT} /Ω	CPE/μF	n	R _{CT} /Ω	CPE/μF	n	R _{CT} /Ω	CPE/μF	n
0.35	3573	60	0.88	1318	138	0.98	2171	82	0.88
0.45	1213	60	0.85	-	-	-	-	-	-
0.55	933	47	0.81	494	138	0.9	534	138	0.87
0.65	4574	47.5	0.79	380	169	0.89	1E20	86	0.83
0.75	-2538	39	0.79	-810	132	0.85	-737	53	0.79
0.85	-1057	40	0.81	-695	140	0.92	-448	50	0.82
0.95	-1690	48	0.82	-511	145	0.91	-266	29	0.75
1.05	-5709	94	0.88	-2264	126	0.85	-363	39	0.77
1.15	1997	97	0.9	1546	210	0.92	-1053	36	0.74

E/V	Pt 30% (2.9 nm)			Pt 40% (3.7 nm)		
	R _{CT} /Ω	CPE/μF	n	R _{CT} /Ω	CPE/μF	n
0.35	4715	54	0.87	3200	11	0.74
0.45	1283	68	0.87	1133	60	0.84
0.55	1764	69	0.85	3970	21	0.82
0.65	-2082	65	0.83	-2618	58	0.84
0.75	-704	37	0.8	-888	24	0.81
0.85	-361	25	0.78	-436	14	0.76
0.95	-233	24	0.76	-255	22	0.80
1.05	-231	15	0.69	-439	25	0.79
1.15	-	-	-	-	-	-

At very low potentials (0.35 V), Nyquist plots showed a large capacitive semicircle, but for clarity, this potential is not show, though the resistance values can be observed in the table 1.

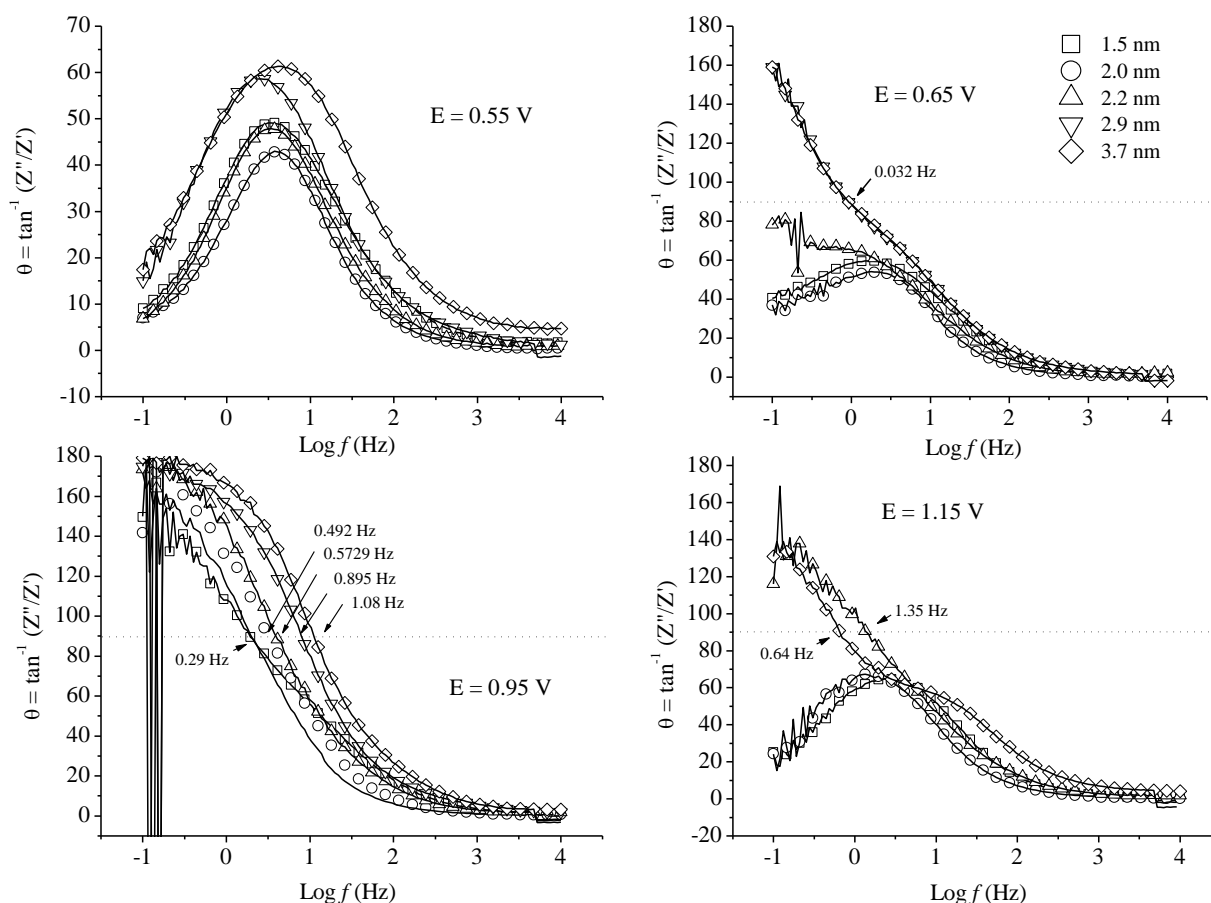


Figure 4. Bode plots for different platinum supported catalysts (size 1.5-3.7 nm) in 1.0 M HCOOH + 0.1 M H₂SO₄ electrolyte solution, at various electrode potentials. The solid lines represent the result of the fitting procedure to the experimental data by the equivalent circuit in Figure 5.

The high charge transfer resistance, in this potential, agrees with that observed in the CV measurements in Figure 2a, where a very low current response related with the accumulation poisonous intermediate species was observed. With further increasing of the electrode potential (0.35

to 0.55 V), the resistive-semicircle diameter decrease, suggesting a small increase in the oxidation process [37]. In agreement with cyclic voltammetry, the smaller particles showed higher activity in this potential range. Weaver et al. through CV and FTIR analysis [31], proposed that higher activity on smaller particles is due to a lower CO coverage. Nevertheless, an explanation of why CO coverage is lower on smaller particles is not well established. Note that before 0.7 V, CO oxidation is very unlikely, and different studies have reported that only a small fraction of CO_{ad} can be removed in the region corresponding to the so-called *pre-peak* [14, 21, 28, 30].

Above 0.65 V, is displayed a transition state represented by a change from the first to the second quadrant in Nyquist plot and angles above 90° in the Bode diagrams spectra. These features concord with the appearance of a NDR, observed by a decrease of the current density in the CV's curves (Figure 2a), and implies a decrease of the reaction rate as potential rinses. The results showed that appearing of NDR take place first on the bigger particles (2.9 to 3.7 nm). Previous reports have proposed that the co-adsorption of the formate ion give a remarkable surface stabilization by *formate-formate* and *formate-CO* interactions, suppressing formic acid oxidation and promoting the appearance of a negative differential resistance (NDR) [38]. Such a consideration, suggests that the potential at which the NDR appears, is directly related to the ability of Pt particles to stabilize the format ion together with CO until reaching what we call "*critical surface concentration*" (CSC), and according to the results, this CSC feature is reached first on the bigger particles.

Above 0.75 V, the appearance of the first HO_{ad} species on the surface detonates the CO_{ad} oxidation reaction, enabling the adsorption of formate ion on platinum sites previously occupied by CO_{ad} . This process results in a dramatic increase in the reaction rate, which can be monitored by a sudden decrease of the charge transfer resistance, until reaching a minimum at 0.95 V, and by a maximum of peak 2 in the voltammograms (Figure 2a). Finally, at potential higher than 0.95 V, the formation of non-reactive oxide species decreases the reaction rate by blocking active sites. Again, it is important to note that, the value of resistance and the change from the second to the first quadrant due to the disappearance of NDR depends on the particle's size. On smaller particles the NDR is suppressed at lower potential, which can be interpreted as follow: *i*) the stabilizing of the formate ions by inter/intramolecular interactions *formate-formate* and *formate-CO* is smaller, and therefore CSC is unlikely; *ii*) smaller particles are more easily oxidized which promote the surface blockage at lower potential avoiding that CSC can be reached. However, further studies must be made to verify these assumptions.

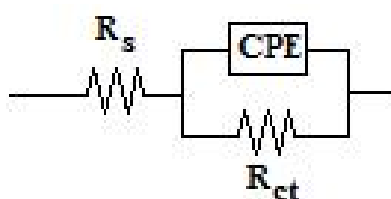


Figure 5. Equivalent circuit for the fitting of EIS spectra during electro-oxidation of formic acid on platinum supported catalysts at several potentials (0.35 – 1.15 V/RHE).

Figure 4 shows the typical Bode plots for carbon supported platinum (1.5-3.7 nm) catalysts in 1.0M HCOOH + 0.1 M H₂SO₄ at different electrode potentials. The kinetic processes of the electrode can also be evaluated from the variation of effective phase angle in relation to the electrode potential and particle size. From 0.35 to 0.55 V, the maximum phase angles remain lower than 90° for all particle size, however at 0.55 V, a slight increase of the maximum may be interpreted as the first sign of preferential formate adsorption onto the surface of larger particles. At 0.65 V, the surface coverage by formate-CO onto the larger particles (2.9-3.7 nm) has reached the CSC condition, which is corroborated by a jump at angles higher than 90° at lower frequencies. This phenomenon corresponds to the transition to negative faradic impedance as shown in the Nyquist plots in Figure 3. At 0.95 V all catalysts show phase angles above 90° due to almost a complete CO and formate oxidation. Note that the frequencies reaching 90° increase with increasing particle size. Finally, further increases of the electrode potential promote the complete removal of CO and the surface oxidation, thus diminishing the number of active sites for adsorption/oxidation of formic acid.

From the impedance results (Figure 3 and 4), the formic acid reaction can be monitored in different potential regions. The equivalent circuit shown in Figure 5, represents the adsorption and charge transfer process of the active species (CO and HCOO, principally) onto the nanoparticle's surfaces, and can be used to fit the impedance data throughout the potential range evaluated. Here, R_s represent the solution resistance which remain unchanged throughout the electrochemical evaluation, R_{CT} is the charge transfer resistance across the double layer due to the faradic reaction, CPE is the constant phase element (CPE) and n is the parameter for CPE which takes values in the range: $0.5 < n < 1$. CPE was used instead of ideal capacitance (C_{dl}) to represent the nonideal behavior of the system [39]. Previous reports have proposed a second time constant [RC] to represent CO oxidation by the appearance of oxygenated species [40], however in our analysis this second component did not represent a major change in the parameter set, so we decided to use only one component which encompasses the adsorption processes and the oxidation reactions of CO and formic acid on the platinum surface.

Table 1 summarizes the fitting results of R_s , R_{ct} , CPE and n at different potentials by using the equivalent circuit represented in Figure 5. From Table 1, it can be seen that the values of solution resistance (R_s) remain invariant within the entire potential range (55-60 Ω). $n \neq 1$ represents the deviation from ideality for a pure capacitance in the interface metal-electrolyte due to the presence of irregularities on the metal surface. On the other hand, it is interesting to note that the charge transfer resistance (R_{ct}) exhibits a clear dependence on electrode potential and particle size. When electrode potential increases from 0.35 to ~ 0.55 or 0.65, depending on particle size, R_{ct} decreased due to the increase of formic acid electro-oxidation. This value of R_{ct} was lower on smaller particles representing higher activity. The transition state (0.65-0.75 V) is always preceded by a significant increase of R_{ct} . This phenomenon was explained by a suppression of reaction rate by a surface stabilization promoted by co-adsorption of formate and CO, which lead to the emergence of a negative differential resistance (NDR), and was more important on bigger particles. Then R_{ct} decrease again because of the promotion of CO and formic acid oxidation and finally increase due to surface oxidation, thus limiting the oxidation of formic acid.

4. CONCLUSIONS

Cyclic voltammetry studies have showed interesting information about formic acid and carbon monoxide oxidation from decomposition of formic acid at very low potential. Contrary to CO oxidation previously adsorbed on Pt surface, the results showed that the overpotential to remove completely CO_{ad} from HCOOH is lower for smaller particles. A well-marked nanoparticles size effect was observed on the electrooxidation of HCOOH, and that under certain conditions smaller particles may have a better catalytic activity than larger ones. During reverse-back sweep after oxidation of CO, there is a significant increase of current density due to electro-oxidation of formic acid on Pt active sites, here the reaction rate is slower on smaller nanoparticles. Results of impedance spectroscopy provide a further insight into the formic acid electro-oxidation processes, and the influence of structural factors, which are correlated with the particle size. In this case, the co-adsorption of formate and CO on Pt has the effect of poisoning the active sites of the catalysts inhibiting the oxidation of formic acid, resulting in a negative differential impedance. This results show that the value of the potential from which the NDR appear, is higher when the size of Pt nanoparticles decrease which can be assigned to differences on structural surface. Indeed, it is well known that nanoparticles oxidize more easily when their size decreases. Some impedance spectra have characteristics that can be attributed to inhibition by the formation of Pt oxide but these results need to be confirmed.

ACKNOWLEDGEMENTS

This work is grateful for his fellowship from CONACYT, SIP-IPN. The authors are also grateful for the financial support from SIP-2010-1029 project and SNI-CONACYT.

References

1. [R. Parsons, T. VanderNoot, *J. Electroanal. Chem.* 9 (1988) 257
2. a) C. Rice, S. Ha, R.I. Masel, P. Waszczuk, A. Wieckowski, T. Barnard, *J. Power Sources*, 111 (2002) 83. b) C. Rice, S. Ha, R.I. Masel, A. Wieckowski, *J. Power Sources*, 115 (2003) 229.
3. a) C. Raghuram, S. Keith, *J. New Mat. Elect. Syst.* 10 (2007) 135. b) S. Uhm, H.J. Lee, J. Lee, *Phys. Chem. Chem. Phys.*, 11 (2009) 9326.
4. R. Young-Woo, S.Y. Ha, R.I. Masel, *J. Power Sources* 117 (2003) 35.
5. A. Capon, R. Parson, *J. Electroanal. Chem.* 44 (1973) 1.
6. A. Capon, R. Parson, *J. Electroanal. Chem.* 44 (1973) 239.
7. A. Miki, S. Ye, M. Osawa, *Chem. Commun.* 14 (2002) 1500.
8. a) M.F. Mrozek, H. Luo, M.J. Weaver, *Langmuir* 16, 8463 (2000). b) M. Shao, A. Peles, k. Shoemaker, *Nano. Lett.*, 11 (2011) 3714.
9. K. Kinoshita, *J. Electrochem. Soc.* 137 (1990) 845.
10. C. Kuhrt, M. Harsdoff, *Surf. Sci.* 245 (1991) 173.
11. J.M. Montejano-Carrizales, F. Aguilera-Granja, J.L. Moran-López, *Nanostruct. Mater.* 8 (1997) 269.
12. M. Arenz, K.J.J. Mayrhofer, V. Stamenkovic, B.B. Blizanac, T. Tomoyuki, P.N. Ross, N.M. Markovic, *J. Am. Chem. Soc.* 127 (2005) 6819.
13. F. Maillard, S. Schreier, M. Hanzlik, E.R. Savinova, S. Weinkauff, U. Stimming, *Phys. Chem. Chem. Phys.* 7 (2005) 385.
14. E. Claude, T. Addou, J.M. Latour, P. Aldebert, *J. Appl. Electrochem.* 28 (1998) 57.

15. J. Clavilier, J.M. Orts, R. Gómez, J.M. Feliu, A. Aldaz, *J. Electroanal. Chem.* 404 (1996) 281.
16. J. Maruyama, I. Abe, *Electrochim. Acta.* 46 (2001) 3381.
17. Y. Takasu, N. Ohashi, X.G. Zhang, Y. Murakami, H. Minagawa, S. Sato, K. Yahikozawa, *Electrochim. Acta.* 41 (1996) 2595.
18. H.A. Gasteiger, S.S. Kocha, B. Sompalli, F.T. Wagner, *Appl. Cat. B* 56 (2005) 9.
19. S. Mukerjee, J. McBreen, *J. Electroanal. Chem.* 448 (1998) 163.
20. K.J.J. Mayrhofer, B.B. Blizanac, M. Arenz, V.R. Stamenkovic, P.N. Ross, N.M. Markovic, *J. Phys. Chem. B* 109 (2005) 14433.
21. T. Chierche, C. Mayer, W.J. Lorenz, *J. Electroanal. Chem.* 135 (1982) 211.
22. H. Kita, T. Katagiri, K. Kunimatsu, *J. Electroanal. Chem.* 220 (1987) 125.
23. H. Okamoto, *Electrochim. Acta* 37 (1992) 37.
24. V.M. Jovanovic, D. Tripkovic, A. Tripkovic, A. Kowal, J. Stoch, *Electrochem. Commun.* 7 (2005) 1039.
25. G. Samjeské, A. Miki, S. Ye, A. Yamakata, Y. Mukouyama, H. Okamoto, M. Osawa, *J. Phys. Chem. B* 109 (2005) 23509.
26. T. Iwasita, *J. Braz. Chem. Soc.* 13 (2002) 401.
27. A. Capon, R. Parsons, *J. Electroanal. Chem.* 44 (1973) 239.
28. Y.X. Chen, S. Ye, M. Heinen, Z. Jusys, M. Osawa, R.J. Behm, *J. Phys. Chem. B* 110 (2006) 9534.
29. K. Kunimatsu, *J. Electroanal. Chem.* 213 (1986) 149.
30. F. Maillard, E.R. Savinova, U. Stimming, *J. Electroanal. Chem.* 599 (2007) 221.
31. S. Park, Y. Xie, M. J. Weaver, *Langmuir* 18 (2002) 5792.
32. S.C. Chang, Y. Ho, M.J. Weaver, *Surf. Sci.* 265 (1992) 81.
33. G. Samjeské, A. Miki, S. Ye, M. Osawa, *J. Phys. Chem. B* 110 (2006) 16559.
34. N.M. Markovic, P.N. Ross Jr, *Surf. Sci. Rep.* 45 (2002) 117.
35. K.A. Friedrich, F. Henglein, U. Stimming, W. Unkauf, *Electrochim. Acta.* 45 (2000) 3283.
36. J.D. Lovic, A.V. Tripkovic, S.Lj. Gojkovic, K.Dj. Popovic, D.V. Tripkovic, P. Olszewski, A. Kowal, *J. Electroanal. Chem.* 581 (2005) 294.
37. Y.C. Liu, X.P. Qiu, W.T. Zhu, G.S. Wu, *J. Power Sources* 114 (2003) 10.
38. Y. Mukouyama, M. Kikuchi, G. Samjeské, M. Osawa, H. Okamoto, *J. Phys. Chem. B*, 110 (2006) 11912.
39. E. Barsoukov, J.R. McDonald, *Impedance spectroscopy: Theory, Experiment and Applications*. Second ed. Wiley-Interscience, New Jersey, 2005, p. 494.
40. W. Chen, J. Kim, S.S. Sun, *Phys. Chem. Chem. Phys.*, 8 (2006) 2779.